

RESEARCH ARTICLE

Fabrication and photocatalytic degradation of reactive blue 19 by CuWO_4 , Ag_3PO_4 , and $\text{CuWO}_4\text{-Ag}_3\text{PO}_4$ composites under visible light irradiation

Aliakbar Arabameri, Mohammad Javad Asadollahzadeh*, Hamed Rashidi, Javad Seyfi

Department of Chemical Engineering, Shahrood Branch, Islamic Azad University, Shahrood, Iran

ARTICLE INFO

Article History:

Received 2021-02-01

Accepted 2021-04-17

Published 2021-05-01

Keywords:

$\text{CuWO}_4\text{-Ag}_3\text{PO}_4$
Composite
Reactive Blue 19
photocatalyst

ABSTRACT

CuWO_4 nano-powder was synthesized via a hydrothermal reaction using $\text{CuCl}_2 \cdot 2\text{H}_2\text{O}$ and $\text{Na}_2\text{WO}_4 \cdot 2\text{H}_2\text{O}$ in the stoichiometric 1:1 Cu:W molar ratio and sodium citrate as raw materials. In addition, Ag_3PO_4 was synthesized by a precipitation method using Na_2HPO_4 and AgNO_3 . Finally, $\text{CuWO}_4\text{-Ag}_3\text{PO}_4$ nanocomposite was synthesized in a precipitation route using the as-synthesized CuWO_4 and Ag_3PO_4 as raw materials. The synthesized materials were characterized by powder X-ray diffraction (PXRD) technique. To investigate the effect of concentration of the basic solutions on the morphology of the obtained materials, the morphologies of the synthesized materials was studied by field emission scanning electron microscopy (FESEM) technique. As shown by the FESEM images, the morphology of CuWO_4 material was spherical particles. Besides, the photocatalytic performance of the as-synthesized nanocomposites was studied for the degradation of Reactive Blue 19 (RB19) under direct visible light irradiation. For the purpose, several reaction parameters affect the degradation yield, such as catalyst amount, pH value and absence/presence of light were investigated. The data showed that the photocatalytic yield at the presence of light irradiation was more when the pH value of the solution was in the acidic range, the weight percent of silver phosphate in the composite mixture was more, and the catalyst amount was more. The findings revealed that a 0.05 g nanocomposite containing 0.24 mmole of Ag_3PO_4 , with an initial pH of 3 and RB 19 volume and concentration of 100 mL and 30 mg/L, respectively, could achieve approximately complete removal after 30 min under visible light illumination.

How to cite this article

Arabameri A., Asadollahzadeh M.J., Rashidi H., Seyfi J. Fabrication and photocatalytic degradation of reactive blue 19 by CuWO_4 , Ag_3PO_4 , and $\text{CuWO}_4\text{-Ag}_3\text{PO}_4$ composites under visible light irradiation. J. Nanoanalysis., 2021; 8(2): 158-166. DOI: 10.22034/jna.008.

INTRODUCTION

Heterogeneous semiconductor photocatalysis for environmental remediation has been actively studied. Copper tungstate (CuWO_4) is belonging to the family of structurally related divalent transition metal tungstates. It contains 3d orbital corresponding to the transition metal [1]. Copper tungstate is a well-known n-type semiconductor that has a wide range of applications as scintillation detectors, photoanodes, laser host, electrode material for photoelectrolysis, optical fibers, solar-assisted water splitting, etc. It can absorb light at

* Corresponding Author Email: m.asadollahzadeh@gmail.com

wavelengths up to 540 nm so has a narrow band gap (E_g) of 2.3–2.4 eV. The electronic properties related to CuWO_4 crystals have been reported in different fields [2-4]. At room temperature and low pressure, the CuWO_4 crystal is an important member of transition metal tungstates which exhibits a triclinic structure [5].

CuWO_4 composites have been widely used for application such as electrical contacts, arc-resistant electrodes, microwave packages, heavy-duty electrical contacts, microelectronics devices, heat sinks materials for high-density integrated circuits, electro-discharge machining, etc. Their

eligibility to serve as such a variety of applications is due to their enhanced mechanical and physical properties, good arc erosion resistance, remarkable thermal and electrical conductivity, and high ability of microwave absorption [6, 7].

Recently, Ag₃PO₄ has attracted considerable attention as a potentially visible light photocatalyst with a band gap of 2.45 eV. So, the role of Ag₃PO₄ is a sensitizer absorbing visible light.[8]. silver phosphate (Ag₃PO₄) crystallizes in a body-centered cubic structure with space group P-43n. This material has received considerable attention because of its photooxidative applications [9]. Ag₃PO₄ exhibits extremely high photooxidative capabilities for O₂ evolution from water splitting as well as organic dye decomposition under visible light irradiation. Ag₃PO₄ has a direct band gap of about 2.43 eV that can absorb energy with a wavelength shorter than about 530 nm. It can achieve a quantum efficiency of approximately 90% at the wavelength of around 420 nm in water oxidation with AgNO₃ as a scavenger [10]. Ag₃PO₄ is the only compound that incorporates nonmetallic p-block specie into Ag₂O [11]. In recent years, silver phosphate (Ag₃PO₄) is a new type of photocatalyst that is highly effective in visible light [12].

One approach to enhance the photocatalytic activity and promote the charge separation efficiency of Ag₃PO₄, is the coupling it with other semiconductors or noble metals. Some coupled systems such as Ag₃PO₄/TiO₂, Ag₃PO₄/AgX (X=Cl, Br, I), Ag₃PO₄/SnO₂, Fe₃O₄/Ag₃PO₄, Ag₃PO₄/Ag, Ag₃PO₄/BiOCl, Ag₃PO₄/reduced graphite oxide sheets, and carbon quantum dots/Ag₃PO₄ composites have recently been developed to improve the photocatalytic activity of Ag₃PO₄ [13]. Besides, there are some other reported composite materials of CuWO₄ and Ag₃PO₄ nanomaterials including Ag₃PO₄-ZnO [9], Ag₃PO₄-GO [14], ZnO/CuWO₄ [15], CdS-CuWO₄-TiO₂ [16], Fe₃O₄/ZnO-CuWO₄ [17], Ag₃PO₄/ZnFe₂O₄ [18].

Several methods have been reported for the synthesis of CuWO₄ nanomaterials including hydrothermal method using Na₂WO₄ and Cu(NO₃)₂·3H₂O at 170 °C for 20 h followed by annealing at 500 °C for 3 h [1], precipitation method [2], ultrasonic method [3, 4], chemical precipitation method [5], hydrolysis method [6], hydrothermal method for synthesizing CuWO₄ film at 180 °C for 8 h followed by annealing at 500 °C for 2 h using H₂N₁₀O₄₁W₁₂·xH₂O and CuCl₂·2H₂O [19], microwave method assisted

solid state method [20], hydrothermal method at 100 °C for 10 h followed by annealing at 500 °C for 2 h using Cu(NO₃)₂ and Na₂WO₄ [21], co-precipitation method [7], hydrothermal method at 110 °C for 2 h followed by annealing at 500 °C using Cu(O₂CCH₃)₂·H₂O and Na₂WO₄·2H₂O as raw materials [15], chemical impregnation method [16], refluxing method [17], hydrothermal method at 180 °C for 18 h followed by annealing at 500 °C using CuCl₂ and Na₂WO₄ as raw materials [22], thermochemical method [23], co-precipitation method [24], hydrothermal method at 180 °C for 28 h followed by annealing at 400 - 700 °C for 2h using Cu(NO₃)₂·3H₂O and Na₂WO₄·2H₂O as raw materials [25], electrochemical method [26, 27], etc. Besides, several methods have been reported for the synthesis of Ag₃PO₄ materials including precipitation method using sodium stearate, AgNO₃ and Na₂HPO₄·12H₂O agitated for 1h [18], co-precipitation method using AgNO₃ and Na₂HPO₄·12H₂O agitated for 1h [8], precipitation method AgNO₃ and Na₂HPO₄·12H₂O agitated for 1h [9], precipitation method using AgNO₃ and Na₂HPO₄·12H₂O [10], precipitation method using NaH₂PO₄, Na₂HPO₄, Na₃PO₄ and AgNO₃ [12], precipitation method using oleic acid, AgNO₃ and H₃PO₄ [13], precipitation method using AgNO₃ and Na₂HPO₄ [14], precipitation method using Ag₂CO₃ and Na₂HPO₄ [28], precipitation method using oleic acid, AgNO₃, Na₂HPO₄ [29] etc.

Anthraquinone-based dyes are more resistant to biodegradation due to their fused aromatic structures compared to azo-based ones [30]. Also, they may cause acute toxicity or even mutagenic effects on exposed aquatic organisms [31]. Therefore, anthraquinone reactive dyes have gradually attracted critical attention from the toxicological and environmental points of view, particularly in light of the current increase in their applications.

Reactive Blue 19 (RB-19) is a commercially representative anthraquinone reactive dye. Few past studies concerning ozonation of RB-19 solution were focused on decolorization efficiency and color removal kinetics [32]. Our previous work has further investigated the transformation of RB-19 under different ozonation conditions in 10 min of reaction time and found that partial oxidation was obtained [33]. Several catalysts have been reported for the photodegradation of RB 19 including K₂S₂O₈ [34], TiO₂ [35], ozonation [36], bacterial flora [37], etc.

In the present work, synthesis of CuWO₄ via hydrothermal method at 180 °C for 18h followed by calcination at 500 °C for 2h using CuCl₂·2H₂O and Na₂WO₄·2H₂O in the stoichiometric 1:1 Cu:W molar ratio as raw materials is reported. Besides, Ag₃PO₄ is prepared by a simple precipitation method at 80 °C for 1 h using Na₂HPO₄ and AgNO₃ as raw materials. In addition, several CuWO₄-Ag₃PO₄ composites with different molar ratios are prepared in the present work. The obtained materials are characterized by PXRD technique. Besides, the morphology of the obtained materials is studied by FESEM images. Moreover, the photocatalytic degradation of RB 19 was investigated under direct visible light irradiation without using H₂O₂. Effects of the reaction parameters such as pH value of dye solution and catalyst amount on the photocatalytic efficiency are also studied.

EXPERIMENTAL

Materials and methods

All chemicals were of analytical grade, obtained from commercial sources, and used without further purification. Phase identifications were performed on a powder X-ray diffractometer D5000 (Siemens AG, Munich, Germany) using CuK_α radiation. The morphology of the obtained materials was examined with a Philips XL30 scanning electron microscope (Philips, Amsterdam, Netherlands). Absorption spectra were recorded on an Analytik Jena Specord 40 (Analytik Jena AG Analytical Instrumentation, Jena, Germany). The concentration of reactive blue 19 was determined at 600 nm using a Shimadzu UV-visible 1650 PC spectrophotometer. A BEL PHS-3BW pH-meter with a combined glass-Ag/AgCl electrode was used for adjustment of the solution pH.

Synthesis of CuWO₄ nanomaterial

In a typical experiment, 2.045 g (0.02 mol) of CuCl₂·2H₂O was added into a 25 mL deionized distilled water contained 100 mL beaker under stirring until the salt was solvated. When the salt was dissolved, 0.29 g (1.0 mmol) of sodium citrate was added to the resultant solution under stirring. The obtained mixture was stirred additionally for 30 min. Then 10 mL deionized distilled water was added to the obtained solution. 6.788 g (0.02 mol) of Na₂WO₄·2H₂O was added to the solution and 5 mL of deionized water was poured to the mixture. The mixture was stirred for 30 min. The obtained final solution was transferred to a Teflon-lined

autoclave. The autoclave was sealed and treated thermally at 180 °C for 18 h. After the desired reaction time, the autoclave was cooled normally to the room temperature. Then the precipitate was filtered and washed with deionized distilled water and ethanol. The final powder was dried at 90 °C for 3h. The obtained dried powder was annealed at 500 °C for 2h. The synthesis yield was 86% for CuWO₄ nanomaterial (S₁).

Synthesis of Ag₃PO₄ nanomaterial

0.3549 g (2.5 mmol) of Na₂HPO₄ and 0.84935g (5 mmol) of AgNO₃ were dissolved in 50 mL of deionized distilled water, separately in two beakers. The obtained solution was stirred for 10 min. The Na₂HPO₄ solution was transferred into a burette. The AgNO₃ was titrated with the Na₂HPO₄ solution (25 drops per min). The titrated solution was then heated at 80 °C for 1h. The obtained precipitate was filtered and washed with deionized distilled water. The final powder was dried at 100 °C for 1h. The synthesis yield was 75% for Ag₃PO₄ nanomaterial (S₂).

Synthesis of CuWO₄-Ag₃PO₄ nanocomposites

a certain amount of CuWO₄ (0.97 g (3.10 mmol) (S₃); 0.95 g (3.05 mmol) (S₄) and 0.9 g (2.89 mmol) (S₅)) was added in an 80 mL of deionized distilled water contained beaker. The mixture was stirred for 90 min. In another beaker containing 5 mL deionized distilled water, a specific amount of Ag₃PO₄ (0.03 g (0.07 mmol); 0.05 g (0.12 mmol); 0.1 g (0.24 mmol)) was added and stirred for 30 min. Afterward, the two beakers were mixed and the obtained solution was heated until it was boiled. Then the solution was refluxed for 90 min. The prepared precipitate was filtered and washed three times with deionized distilled water. The obtained powder was dried at 90 °C for 3 h.

RESULTS AND DISCUSSION

Characterization

The X-ray diffraction patterns of the CuWO₄ (S₁) and Ag₃PO₄ (S₂) are reported in Fig. 1. Besides, the XRD patterns of the obtained composites (S₃, S₄ and S₅) are reported in Fig. 2. The results show that the patterns for S₁ and S₂ have a main CuWO₄ crystal structure with space group P-1. Lattice parameters were found as a = 4.87 Å, b = 5.82 Å and c = 4.68 Å with α = 88.35°, β = 92.50° and γ = 97.20° [1-5]. Besides, the PXRD pattern of S₃ shows that Ag₃PO₄ crystallizes in the cubic crystal system with

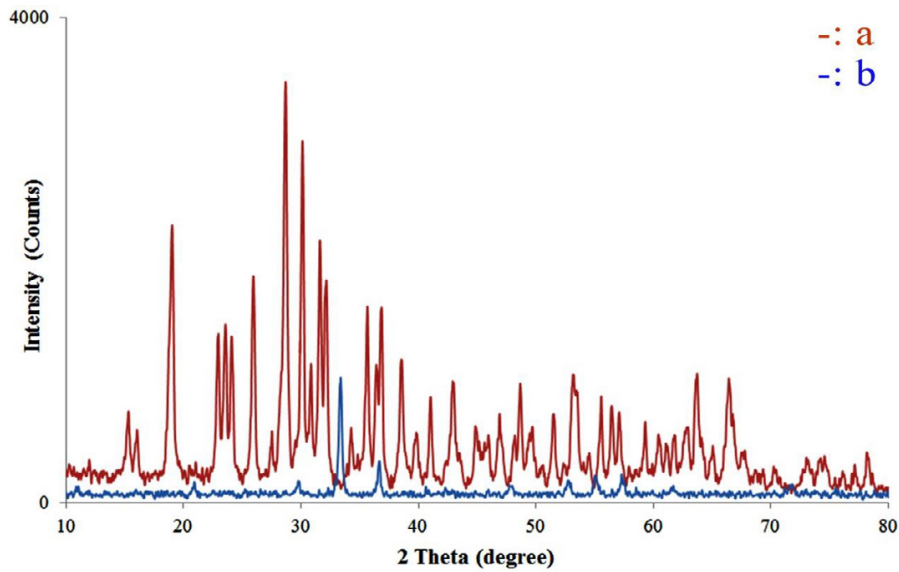


Fig. 1. PXRD patterns of a) S_1 and b) S_2 .

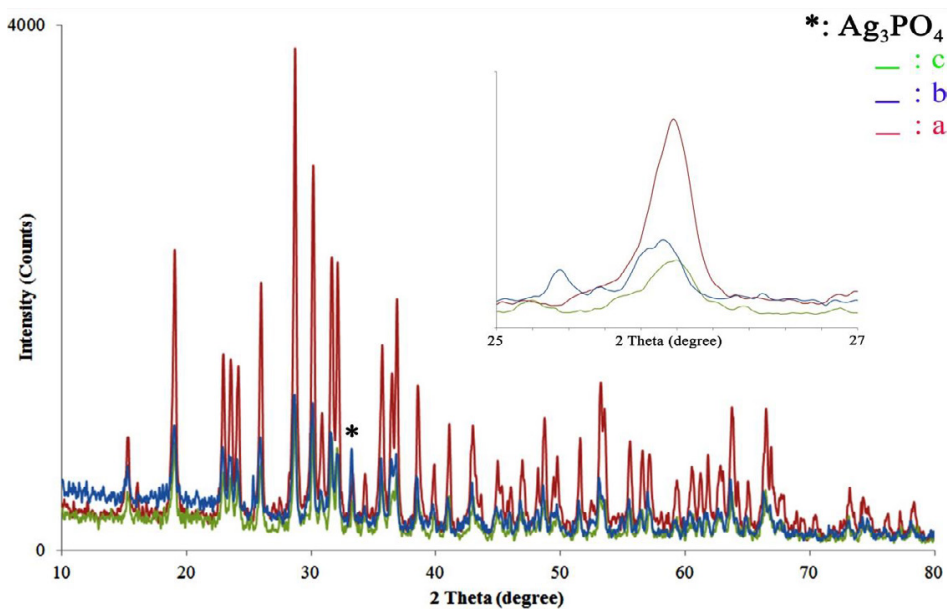


Fig. 2. PXRD patterns of a) S_3 , b) S_4 and c) S_5 .

space group P-43n. The lattice parameters were found as $a = b = c = 5.99 \text{ \AA}$ [8-13].

Fig. 2 shows the PXRD patterns of S_3 to S_5 . It was found that the crystal phase growth was decreased with increasing the Ag_3PO_4 ratio to CuWO_4 in the composite material. Besides, the inset image in Fig. 2 confirms the conclusion. Besides, it shows that when the weight percent of Ag_3PO_4 was increased from 3% (S_3) to 5% (S_4), the peak shifts toward lower 2θ value. It shows that there is an expansion

in the crystal system; but when increasing the Ag_3PO_4 value to 10% (S_5), the peak shifts toward higher 2θ value. Therefore, there is a contraction in the unit cell.

Fig. 3 shows the FESEM images of $S_1 - S_5$ nanomaterials. The image of CuWO_4 nanomaterial showed that the morphology of the obtained material was a spherical particle with highly homogeneous morphology (a). The FESEM image of the synthesized Ag_3PO_4 nanomaterial showed

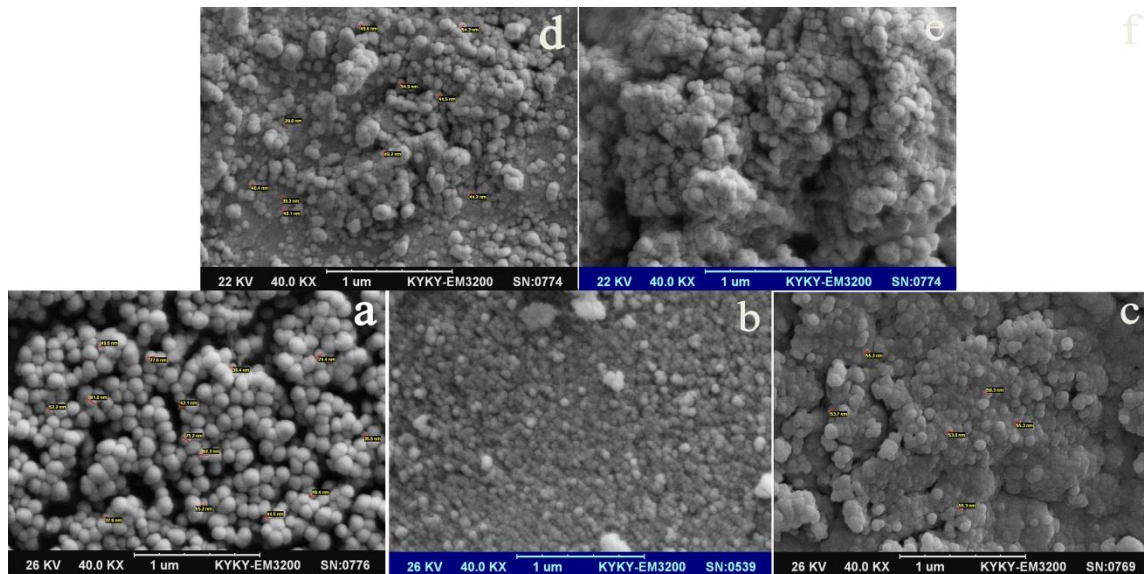


Fig. 3. FESEM images of a) S_1 , b) S_2 , c) S_3 , d) S_4 and e) S_5 .

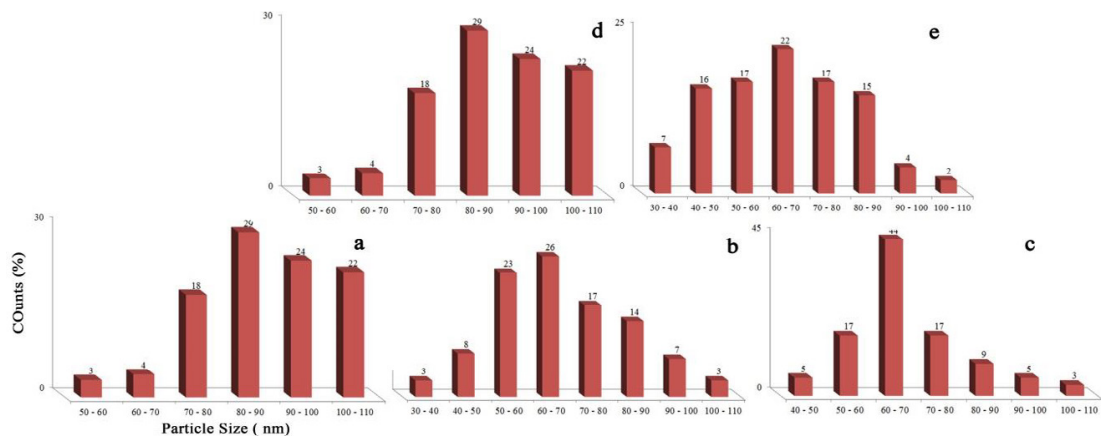


Fig. 4. Particle size distribution profiles of a) S_1 , b) S_2 , c) S_3 , d) S_4 and e) S_5 .

that the morphology of the target was particles with homogeneous morphology (b). Fig. 3 d-f shows the FESEM images of $S_3 - S_5$. The images show that the morphology of the targets was changed with increasing the weight percent of Ag_3PO_4 in the composite mixture. It was found that the morphology of the target was highly homogeneous spherical particles when the weight percent were 3 and 5 %. However, the morphology of the target was changed to particles in which the morphology of the targets was heterogeneous.

Fig. 4 a - f shows the particle size distribution profiles of $S_1 - S_5$, respectively. The data for the size distribution of CuWO_4 showed that the maximum

particle diameter is in the range of 80 - 90 nm For Ag_3PO_4 , it can be seen the high homogeneity of the size of the particles and the maximum size range was 60 - 70 nm. Fig. 4 c - e shows the data for the composite nanomaterials. The data indicate that the maximum diameter sizes were about 80 - 90, 60 - 70 and 60 - 70 nm for S_3 , S_4 and S_5 , respectively. The average particle sizes were decreased with increasing Ag_3PO_4 weight percent in the composite material.

Photocatalytic activity

The photocatalytic activity of the synthesized samples was investigated for the degradation of

RB 19 (Anthraquinone dye) under direct visible light irradiation. A light filter was used to prevent wavelengths below 400 nm. To prepare a 30 ppm RB 19 dye solution, 0.03 g of RB 19 powder was dissolved in 1000 mL of deionized water. The pH value of the dye solution was adjusted to the desired amount using 1M of HCl or NaOH solutions. In a typical photocatalytic process under the visible light irradiation, a certain amount (g) of the synthesized sample was added into 100 mL of the as-prepared MB solution and sonicated for 10 min in a dark room to establish an adsorption/desorption equilibrium between RB 19 molecules and the surface of the photocatalyst followed by further magnetic stirring (250 rpm) under direct visible light irradiation. The solution was drawn out at the certain time and the photocatalyst was separated by centrifugation to measure the absorption spectra of RB 19 and calculate the RB 19 concentration using UV-Vis spectrophotometry. The photodegradation yield (%) of RB 19 was calculated by the following formula:

$$\left(\frac{A_0 - A_t}{A_0} \right) \times 100$$

Where, A₀ and A_t represent the initial absorbance of RB 19 at 602 nm and the absorbance at time t, respectively.

To study the degradation of RB 19 in a dark room under the typical catalytic degradation process,

some tests were done. Fig. 5 a and b presents the degradation of RB 19 using the synthesized samples and in different pH values, respectively, under dark condition. The data in Fig. 5 a indicates that there was no considerable degradation in the dark room. Besides, Fig. 5 b reveals that by changing the pH value from acidic to basic condition, the degradation of RB 19 decreased. However, the degradation percent was still low under the dark condition. So, it can be concluded the degradation yield under dark room for the samples in any solution pH was not considerable.

The results in photocatalytic degradation of RB 19 under direct visible light irradiation. shows that the degradation yield of the as-prepared nanomaterials was increased by increasing Ag₃PO₄ weight percent in the nanocomposite mixture (Fig. 6 a) . It was found that under direct visible light irradiation when the catalyst weight in the reaction mixture was increased, the considerable higher degradation yield of RB 19 can be achieved , it can be concluded that the surface area exists for the dye to adsorb on the surface of the catalyst was increased and so the degradation in the certain time was done faster. However, it is clear that 0.03 g of catalyst in the reaction mixture can be the optimum value.

Fig. 7 a and b presents the effect of the solution pH value on the degradation yield under the visible light irradiation. Fig. 7 a indicates that when the pH value was in the acidic range, the

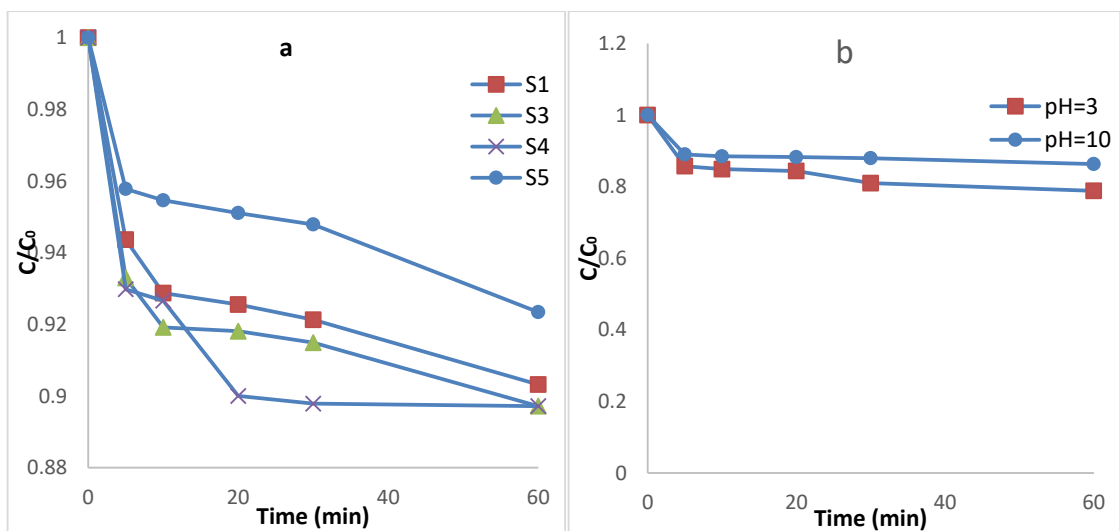


Fig. 5. Plots of the photodegradation of RhB at the dark room (a) the degradation efficiency for different nanocomposites (Reaction condition: pH= 6, 100 mL of 30 ppm dye solution and 0.05 g of catalyst) and (b) the effect of solution pH value on the degradation yield for the reference composite s₃ (Reaction condition: 100 mL of 30 ppm dye solution and 0.05 g of catalyst).

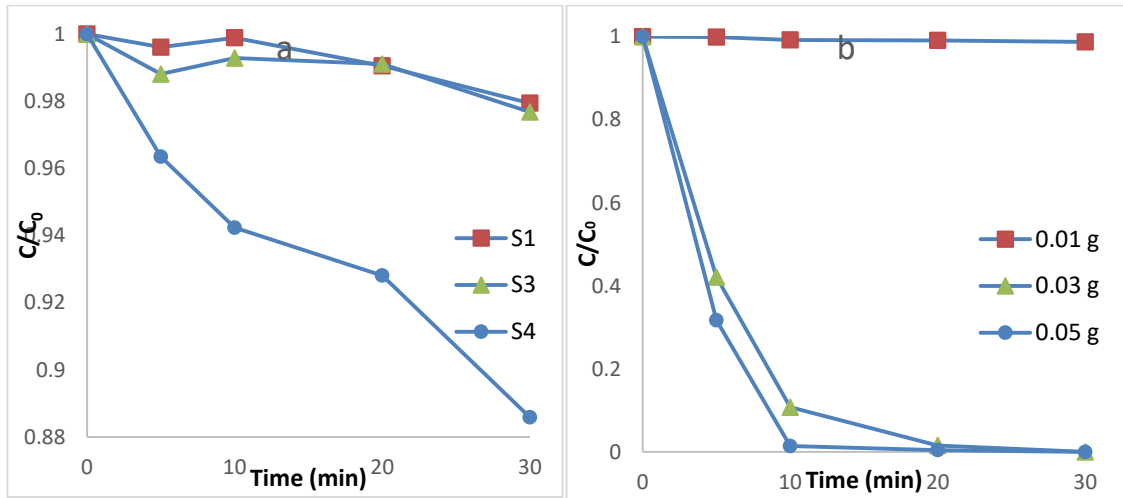


Fig. 6. Plots of the photodegradation of RhB under direct visible light irradiation (a) degradation yield for the synthesized nanocomposites (Reaction condition: 0.03 g of catalyst, pH=6, 100 mL of 30 ppm dye solution) and (b) effect of catalyst amount on the degradation yield for the reference composite S_5 (Reaction condition: pH=3, 100 mL of 30 ppm dye solution).

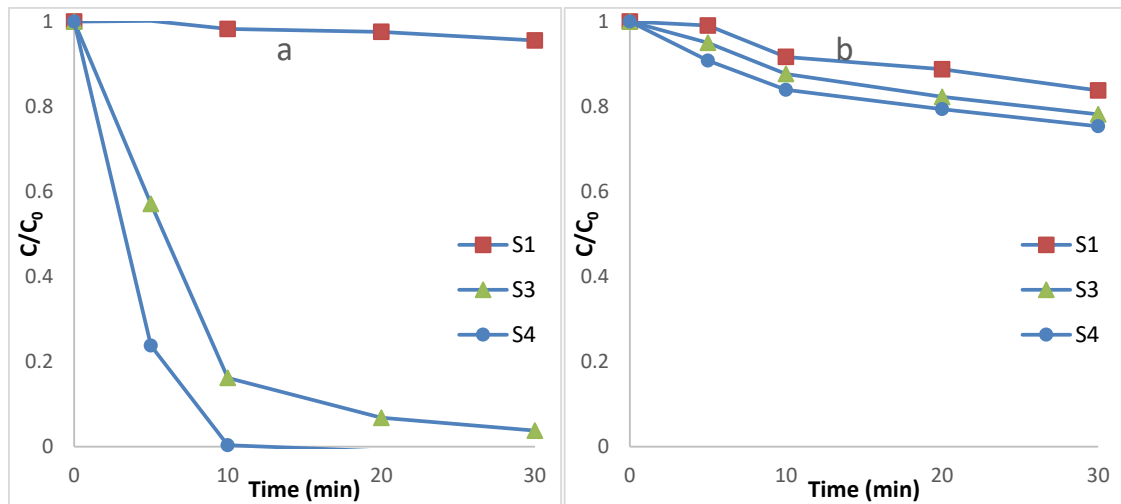


Fig. 7. Efficiency of degradation yield of the as-synthesized nanomaterials when (a) the pH value is 3 and (b) the pH value is 10. (Reaction condition: 0.03 g of catalyst, 100 mL of 30 ppm dye solution).

degradation yield increased for the samples in which the weight percent of Ag_3PO_4 was more. The observation indicates that existing H^+ in the solution activated the oxidizing agents and thus the degradation was done faster. Fig. 7 b shows that when the solution pH value was in the basic range, the degradation yield of all of the samples decreased considerably. Besides, we have mentioned in Fig. 6 a that when the pH

value of the solution was in the neutral range, the degradation yield is low. However, it is clear that the yield is more for the sample in which the weight percent of Ag_3PO_4 is more (S_4). So, we can conclude that the pH=3 is the optimum value.

Fig. 8 a and b presents the UV-Vis spectra and calibration diagram of the as-prepared RB 19 dye solution. The data reveal that there is no sensitive error in the preparation process of the dye solutions.

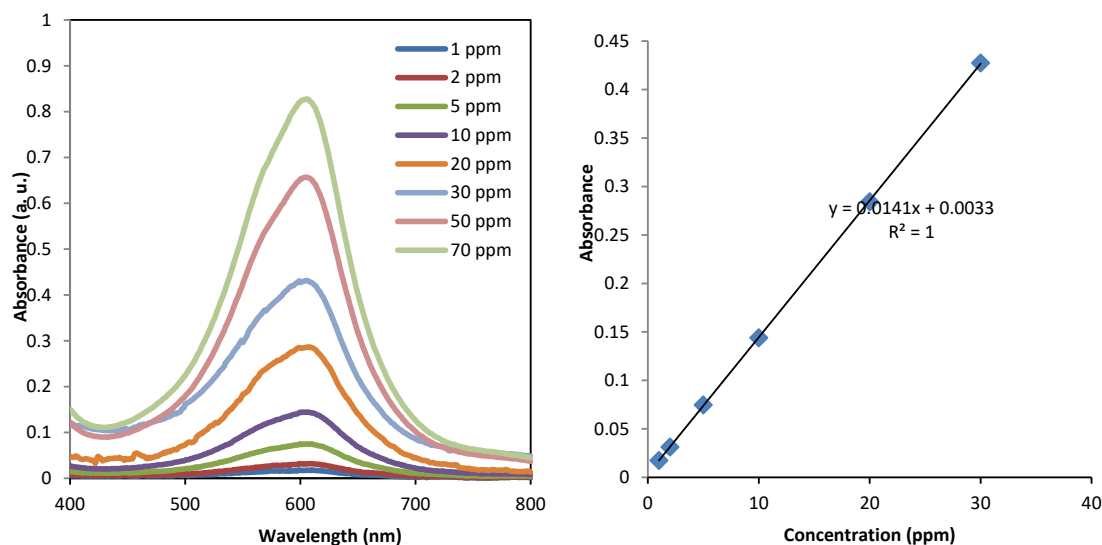


Fig. 8. Plots of a) UV-Vis spectra of RhB solutions and b) calibration curve of the as-prepared solutions.

CONCLUSION

This study described the hydrothermal and precipitation syntheses of highly crystalline CuWO₄, Ag₃PO₄ and CuWO₄-Ag₃PO₄ nanomaterials. The PXRD patterns indicated that the targets were crystallized well in triclinic (CuWO₄) and cubic (Ag₃PO₄) crystal systems. The patterns showed that the unit cells were expanded by increasing Ag₃PO₄ weight ratio in the composite mixture. The particle size distribution data showed that the diameter size ranges were decreased considerably by increasing the Ag₃PO₄ weight percent in the synthesized nanocomposite. FESEM images showed that Ag₃PO₄ weight percent for the synthesis of composite materials has a main effect on the synthesis of CuWO₄-Ag₃PO₄ nanocomposites. The RB 19 photocatalytic degradation data revealed that a 0.05 g nanocomposite containing 0.24 mmole of Ag₃PO₄, with an initial pH of 3 and rhodamine B volume and concentration of 100 mL and 30 mg/L, respectively, could achieve removal of 100 % after 30 min under visible light illumination without using H₂O₂.

CONFLICT OF INTEREST

The authors declare that there is no conflict of interests regarding the publication of this manuscript.

REFERENCE

- Chen H, Leng W, Xu Y. Enhanced Visible-Light Photoactivity of CuWO₄ through a Surface-Deposited CuO. *The Journal of Physical Chemistry C*. 2014;118(19):9982-9.
- Xiong X, Chen H, Xu Y. Improved Photocatalytic Activity of TiO₂ on the Addition of CuWO₄. *The Journal of Physical Chemistry C*. 2015;119(11):5946-53.
- Dutta DP, Rathore A, Ballal A, Tyagi AK. Selective sorption and subsequent photocatalytic degradation of cationic dyes by sonochemically synthesized nano CuWO₄ and Cu₃Mo₂O₉. *RSC Advances*. 2015;5(115):94866-78.
- Pourmortazavi SM, Rahimi-Nasrabadi M, Khalilian-Shalamzari M, Ghaeni HR, Hajimirsadeghi SS. Facile Chemical Synthesis and Characterization of Copper Tungstate Nanoparticles. *Journal of Inorganic and Organometallic Polymers and Materials*. 2013;24(2):333-9.
- Hosseinpour-mashkani SM, Sobhani-Nasab A. Simple synthesis and characterization of copper tungstate nanoparticles: investigation of surfactant effect and its photocatalyst application. *Journal of Materials Science: Materials in Electronics*. 2016;27(7):7548-53.
- Chen H, Xiong X, Hao L, Zhang X, Xu Y. Improved visible light photocatalytic activity of WO₃ through CuWO₄ for phenol degradation. *Applied Surface Science*. 2016;389:491-5.
- Hashempour M, Razavizadeh H, Rezaie H-R, Hashempour M, Ardestani M. Chemical mechanism of precipitate formation and pH effect on the morphology and thermochemical co-precipitation of W-Cu nanocomposite powders. *Materials Chemistry and Physics*. 2010;123(1):83-90.
- Botelho G, Sczancoski JC, Andres J, Gracia L, Longo E. Experimental and Theoretical Study on the Structure, Optical Properties, and Growth of Metallic Silver Nanostructures in Ag₃PO₄. *The Journal of Physical Chemistry C*. 2015;119(11):6293-306.
- Dong C, Wu K-L, Li M-R, Liu L, Wei X-W. Synthesis of Ag₃PO₄-ZnO nanorod composites with high visible-light photocatalytic activity. *Catalysis Communications*. 2014;46:32-5.
- Chen X, Dai Y, Wang X. Methods and mechanism for improvement of photocatalytic activity and stability of Ag₃PO₄: A review. *Journal of Alloys and Compounds*.

- 2015;649:910-32.
11. Ma Y-z, Cheng F, Liu W-s, Wang J, Wang Y-k. Research progress of Ag₃PO₄-based photocatalyst: Fundamentals and performance enhancement. *Transactions of Nonferrous Metals Society of China*. 2015;25(1):112-21.
 12. Amornpitoksuk P, Intarasuwan K, Suwanboon S, Baltrusaitis J. Effect of Phosphate Salts (Na₃PO₄, Na₂HPO₄, and NaH₂PO₄) on Ag₃PO₄ Morphology for Photocatalytic Dye Degradation under Visible Light and Toxicity of the Degraded Dye Products. *Industrial & Engineering Chemistry Research*. 2013;52(49):17369-75.
 13. Dong P, Yin Y, Xu N, Guan R, Hou G, Wang Y. Facile synthesis of tetrahedral Ag₃PO₄ mesocrystals and its enhanced photocatalytic activity. *Materials Research Bulletin*. 2014;60:682-9.
 14. Chen X-j, Dai Y-z, Wang X-y, Guo J, Liu T-h, Li F-f. Synthesis and characterization of Ag₃PO₄ immobilized with graphene oxide (GO) for enhanced photocatalytic activity and stability over 2,4-dichlorophenol under visible light irradiation. *Journal of Hazardous Materials*. 2015;292:9-18.
 15. Mavrič T, Valant M, Forster M, Cowan AJ, Lavrenčič U, Emin S. Design of a highly photocatalytically active ZnO/CuWO₄ nanocomposite. *Journal of Colloid and Interface Science*. 2016;483:93-101.
 16. Vignesh K, Priyanka R, Hariharan R, Rajarajan M, Suganthi A. Fabrication of CdS and CuWO₄ modified TiO₂ nanoparticles and its photocatalytic activity under visible light irradiation. *Journal of Industrial and Engineering Chemistry*. 2014;20(2):435-43.
 17. Shekofteh-Gohari M, Habibi-Yangjeh A. Fabrication of novel magnetically separable visible-light-driven photocatalysts through photosensitization of Fe₃O₄/ZnO with CuWO₄. *Journal of Industrial and Engineering Chemistry*. 2016;44:174-84.
 18. Chen X, Dai Y, Huang W. Novel Ag₃PO₄/ZnFe₂O₄ composite photocatalyst with enhanced visible light photocatalytic activity. *Materials Letters*. 2015;145:125-8.
 19. Tang Y, Rong N, Liu F, Chu M, Dong H, Zhang Y, et al. Enhancement of the photoelectrochemical performance of CuWO₄ films for water splitting by hydrogen treatment. *Applied Surface Science*. 2016;361:133-40.
 20. Dhilip Kumar R, Karuppuchamy S. Microwave-assisted synthesis of copper tungstate nanopowder for supercapacitor applications. *Ceramics International*. 2014;40(8):12397-402.
 21. Wei C, Huang Y, Zhang X, Chen X, Yan J. Soft-template hydrothermal synthesis of nanostructured Copper(II) Tungstate cubes for Electrochemical Charge Storage Application. *Electrochimica Acta*. 2016;220:156-63.
 22. Liang L, Liu H, Tian Y, Hao Q, Liu C, Wang W, et al. Fabrication of novel CuWO₄ hollow microsphere photocatalyst for dye degradation under visible-light irradiation. *Materials Letters*. 2016;182:302-4.
 23. Hashempour M, Razavizadeh H, Rezaie HR, Salehi MT. Thermochemical preparation of W-25%Cu nanocomposite powder through a CVT mechanism. *Materials Characterization*. 2009;60(11):1232-40.
 24. ReddyPrasad P, Naidoo EB. Ultrasonic synthesis of high fluorescent C-dots and modified with CuWO₄ nanocomposite for effective photocatalytic activity. *Journal of Molecular Structure*. 2015;1098:146-52.
 25. Ma D, Xie J, Li J, Liu S, Wang F, Zhang H, et al. Synthesis and hydrogen reduction of nano-sized copper tungstate powders produced by a hydrothermal method. *International Journal of Refractory Metals and Hard Materials*. 2014;46:152-8.
 26. Pourmortazavi SM, Rahimi-Nasrabadi M, Fazli Y, Mohammad-Zadeh M. Taguchi method assisted optimization of electrochemical synthesis and structural characterization of copper tungstate nanoparticles. *International Journal of Refractory Metals and Hard Materials*. 2015;51:29-34.
 27. Zhang W, Yin J, Min F, Jia L, Zhang D, Zhang Q, et al. Cyclic voltammetry analysis of copper electrode performance in Na₂WO₄ solution and optical property of electrochemical synthesized CuWO₄ nanoparticles. *Journal of Alloys and Compounds*. 2017;690:221-7.
 28. Wan J, Sun L, Fan J, Liu E, Hu X, Tang C, et al. Facile synthesis of porous Ag₃PO₄ nanotubes for enhanced photocatalytic activity under visible light. *Applied Surface Science*. 2015;355:615-22.
 29. Wang N, Zhou Y, Chen C, Cheng L, Ding H. A g-C₃N₄ supported graphene oxide/Ag₃PO₄ composite with remarkably enhanced photocatalytic activity under visible light. *Catalysis Communications*. 2016;73:74-9.
 30. Deng D, Guo J, Zeng G, Sun G. Decolorization of anthraquinone, triphenylmethane and azo dyes by a new isolated *Bacillus cereus* strain DC11. *International Biodeterioration & Biodegradation*. 2008;62(3):263-9.
 31. Novotný Ć, Dias N, Kapanen A, Malachová K, Váňdrovcová M, Itävaara M, et al. Comparative use of bacterial, algal and protozoan tests to study toxicity of azo- and anthraquinone dyes. *Chemosphere*. 2006;63(9):1436-42.
 32. Hsu Y-C, Chen Y-F, Chen J-H. Decolorization of Dye RB-19 Solution in a Continuous Ozone Process. *Journal of Environmental Science and Health, Part A*. 2004;39(1):127-44.
 33. Fanchiang JM, Tseng DH. Decolorization and transformation of anthraquinone dye Reactive Blue 19 by ozonation. *Environmental Technology*. 2009;30(2):161-72.
 34. Rezaee, A., et al., *Photochemical oxidation of reactive blue 19 dye (RB19) in textile wastewater by UV/K₂S₂O₈ process*. *Journal of Environmental Health Science & Engineering*, 2008. 5(2): p. 95-100.
 35. Abu Bakar F, Ruzicka J-Y, Nuramdhani I, Williamson BE, Holzenkaempfer M, Golovko VB. Investigation of the Photodegradation of Reactive Blue 19 on P-25 Titanium Dioxide: Effect of Experimental Parameters. *Australian Journal of Chemistry*. 2015;68(3):471.
 36. Fanchiang J-M, Tseng D-H. Degradation of anthraquinone dye C.I. Reactive Blue 19 in aqueous solution by ozonation. *Chemosphere*. 2009;77(2):214-21.
 37. Xie X, Zheng X, Yu C, Zhang Q, Wang Y, Cong J, et al. Highly efficient biodegradation of reactive blue 19 under the activation of tea residue by a newly screened mixed bacterial flora DDMY2. *RSC Advances*. 2019;9(43):24791-801.